A Journal of the Gesellschaft Deutscher Chemiker

Angewandte International Edition GDCh Chemie

www.angewandte.org

Accepted Article

Title: Highly Mesoporous Metal Organic Frameworks as Synergistic Multimodal Catalytic Platforms for Divergent Cascade Reactions

Authors: Soumen Dutta, Nitee Kumari, Sateesh Dubbu, Sun Woo Jang, Amit Kumar, Hiroyoshi Ohtsu, Junghoon Kim, Masaki Kawano, Seung Hwan Cho, and In Su Lee

To be cited as: *Angew. Chem. Int. Ed.* 10.1002/anie.201916578
Angew. Chem. 10.1002/ange.201916578

Link to VoR: http://dx.doi.org/10.1002/anie.201916578
http://dx.doi.org/10.1002/ange.201916578

WILEY-VCH

10.1002/anie.201916578

WILEY-VCH

COMMUNICATION

Highly Mesoporous Metal Organic Frameworks as Synergistic Multimodal Catalytic Platforms for Divergent Cascade Reactions

Soumen Dutta,[a,b] Nitee Kumari,[a,b] Sateesh Dubbu,[a,b] Sun Woo Jang,[a,b] Amit Kumar,[a,b] Hiroyoshi Ohtsu,[c] Junghoon Kim,[b] Seung Hwan Cho,[b] Masaki Kawano,[c] and In Su Lee*[a,b]

Abstract: Rational engineering and assimilation of diverse chemo- and bio-catalytic functionalities in single nanostructure is highly desired for efficient multi-step chemical reactions but remain an elusive task in synthetic nanoscience. Here, we design and synthesize mesoporous metal organic framework (MOF)-based multimodal catalytic nanoreactors (MCNRs) consisting of customizable different metal nanocrystals in a spatio-selective manner, stably anchored enzymes in mesopores and coordinatively unsaturated metal cationic MOF-nodes, all within the single nanoreactor space. Such highly intimate and diverse catalytic mesoporous microenvironment and facile active-site accessibility in MCNR affected one-pot multi-step cascade reactions involving heterogeneous catalytic nitro-aldol reaction followed by [Pd/lipase]-catalyzed chemoenzymatic dynamic kinetic resolution yielding optically pure (ee > 99%) nitroalcohol derivatives in quantitative yields by the co-operative and synergistic participation from different chemo-bio-catalytic components.

The high efficiency of biochemical reactions leading to the synthesis and assembly of biomolecules, is attributed to the nature's extensive use of cascade chemistry.[1] In chemical and pharmaceutical manufacturing, the bio-inspired multi-module cascade catalysis which combine the reactivity, selectivity and robustness of natural enzymes together with synthetic catalysts are highly desired which can circumvent tedious workups, the intermediate-decomposition and the time and cost; however, the reaction parameters of different catalysts usually deactivate either of the catalysts during the cascade process.[2] The rational integration of different catalysis modules into single hybrid nanoarchitecture without compromising their reactivity and stability are challenging due to the difference in their structure, size, composition, surface chemistry, and active-site reactivity. So far, several strategies have emerged to integrate natural enzymes with synthetic catalysts using supports such as mesoporous silica,[3a] metal-organic frameworks (MOFs),[3b] reduced graphene oxide,[3c] and polymeric matrices,[3d] where the compatibility between carriers and enzymes, insufficient exposure of active sites, low reactivity of heterogeneous phase under ambient conditions and poor molecular transport still remain as main hurdles in their usage in divergent cascade reactions.[4]

Hybrid structures having MOFs as crystalline porous well-enginearable nano-housing composed of designer inorganic nodes (ions or clusters) and organic ligands, can accommodate variety of metal nanocrystals (NCs)[5] or biomolecules[6] at the interior defective sites and have found many applications in catalysis, biosensing, therapy, molecular delivery and energy-conversion. The enormous design adaptability of pore geometries having unique chemical functionality with high pore volume of MOFs,[7] can simultaneously allow judicious allocation of catalytic metal NCs and also efficiently intake guest enzyme at the desired MOF-sites, protecting them from deactivation[8] concomitantly generating the catalytic unsaturated inorganic metal sites.[9] However, size incompatibility of bulky enzymes and NCs with much smaller gateway pores of MOF-exteriors results in their restricted diffusion-mediated assembly through conventional pore entrapment method,[10] therefore, triggering the need of synthesizing hierarchically meso- and micro-porous MOFs as host matrix,[11] which may overcome low enzyme loading efficiency and slow flux rate of reactants, where enzyme ingress into the large pores easily accessible to the substrates, while its small pores offer the selective pathway for intermediates/reactants/ products. Here, we introduce design synthesis and application of multimodal catalytic nanoreactors (**MCNRs**) for realizing divergent cascade reactions involving heterogeneous and biocatalytic steps, by ingeniously assimilating three catalytic counterparts: metal NCs, enzyme-biocatalysts and intra-MOF coordinatively unsaturated metal cationic nodes as heterogenized homogeneous catalysts within *in situ* generated metal organic-mesopores (Scheme 1). As the key step for the synthesis of MCNRs, we exploited polyvinylpyrrolidone (PVP), an amphiphilic non-ionic polymer, for the generation of mesopores (>20 nm) during the crystallization of cobalt-based zeolitic imidazolate frameworks (**ZIF67**) *via* a transient competitive coordination chemistry and massive evolution of unsaturated metal sites.

In a typical procedure to synthesize defect-rich metal nodes in porous **ZIF67** (**DP-ZIF67**), PVP was added as metal-coordinating bulky polymer during the formation of **ZIF67**-domains to induce partial disruption of imidazole-Co(II) catenation process and generate high mesoporosity in the resulting **DP-ZIF67** crystals. The transmission electron microscopy (TEM) images of **DP-ZIF67** showed typical rhombic dodecahedron morphology similar to pristine **ZIF67** with *ca.* 800 nm size, having contrast gradient throughout all the crystals, signifying the presence of large pores (20-40 nm) (Figure 1a, S1a, S4). Further, the field emission scanning electron microscope (FE-SEM) images of the **DP-ZIF67** revealed the roughened surface of the crystals and presence of open pores, which was also authenticated from high-angle annular dark-field scanning TEM (HAADF-STEM) images (Figure 2b-c, S1b). Additionally, the

[a] Dr. S. Dutta, Dr. N. Kumari, Dr. S. Dubbu, S. W. Jang, Dr. A. Kumar, Prof. I. S. Lee
Center for Nanospace-confined Chemical Reactions (NCCR), Pohang University of Science and Technology (POSTECH), Pohang 37673, South Korea
E-mail: insulee97@postech.ac.kr (I. S. L.)

[b] Dr. S. Dutta, Dr. N. Kumari, Dr. S. Dubbu, S. W. Jang, Dr. A. Kumar, J. Kim, Prof. S. H. Cho, Prof. I. S Lee
Department of Chemistry, Pohang University of Science and Technology (POSTECH), Pohang 37673, South Korea

[c] Dr. H. Ohtsu, Prof. M. Kawano
Department of Chemistry, School of Science, Tokyo Institute of Technology, Tokyo 152-8550, Japan

Supporting information for this article is given via a link at the end of the document.

10.1002/anie.201916578
WILEY-VCH

COMMUNICATION

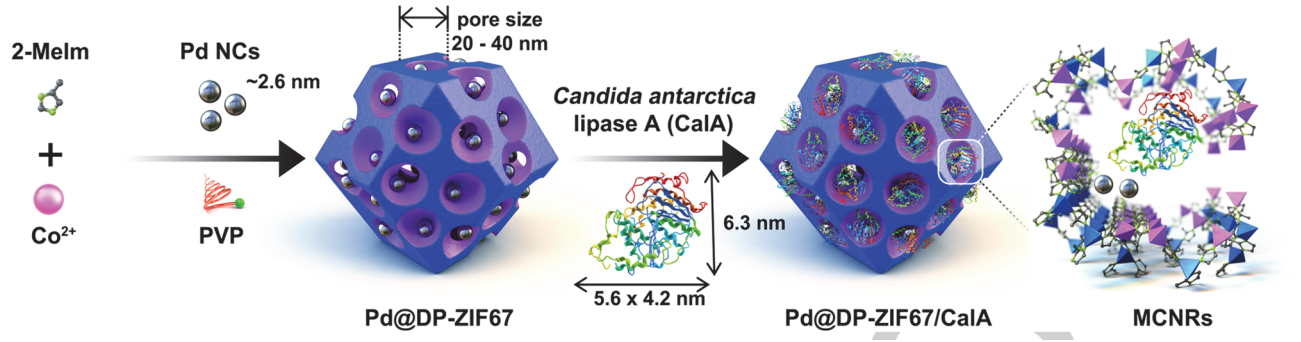

Scheme 1. Synthetic strategy towards multimodal catalytic nanoreactors (MCNRs) containing coordinately unsaturated Co^{2+} (violet colored metal sites), Pd NCs and CalA inside DP-ZIF67.

focused ion beam-slicing followed by TEM (FIB-TEM) revealed numerous hexagonal nanoplates (~600–800 nm) containing randomly distributed mesopores (average size = 30±9 nm), endorsing the consistent mesoporous channels reaching even to the core-region of the **DP-ZIF67** (Figure 1d). In X-ray diffraction (XRD) analysis the characteristic peaks of **DP-ZIF67** confirmed the original framework structure of **ZIF67** having high crystallinity (Inset; Figure 1e). In Brunauer–Emmett–Teller (BET) measurements, the vertical N_2-sorption isotherm at relatively low P/P_0 for **DP-ZIF67** and **ZIF67** (Figure S3) exhibited the intrinsic microporous structures for both the materials, however, H_4 hysteresis loop in P/P_0 = 0.4–0.8 range implied the additional presence of mesopores for only **DP-ZIF67**, also the BET surface area of **DP-ZIF67** and **ZIF67** were found to be 1654 and 1672 $m^2 g^{-1}$, respectively; in addition, the Barrett–Joyner–Halenda (BJH) size distribution plot also verified the presence of mesopores having diameters centered at 22 and 40 nm (Figure 1e) in **DP-ZIF67**. When the synthesis of **DP-ZIF67** was attempted without using any PVP, it could only generate the solid **ZIF67** with no mesoporosity (Figure S5), evidently suggesting possible coordination modulation of Co(II) sites by bulky sized metallophillic PVP polymers which is critical for the generation of large sized mesopores in **DP-ZIF67**.[11b] Notably, for generating the desired mesoporosity, optimum amount of PVP with respect to Co(II) was required (350 mg of PVP for 0.5 mmol of Co^{2+} ions) as lower amount of PVP could not generate any mesopores and larger amounts of PVP slowed down the formation of MOF (Figure S7).

Further, to identify any PVP-induced chemical change in the coordination environment of metal sites, X-ray photoelectron spectrum (XPS) for Co 2p and N 1s of **ZIF67** and **DP-ZIF67** were analyzed (Figure S8). In comparison to the pristine **ZIF67**, significant broadening of XPS peaks for both Co and N was observed for **DP-ZIF67** confirming the changed coordination behaviors of Co (Figure S8c, d) — the typical peaks at 781.1 and 797.0 eV in the Co 2p spectra are attributed to Co $2p_{3/2}$ and Co $2p_{1/2}$, respectively, corresponding to the fully tetra-coordinated Co(II)-N_4 system (Figure 1f); the other pair of peaks at 779.9 and

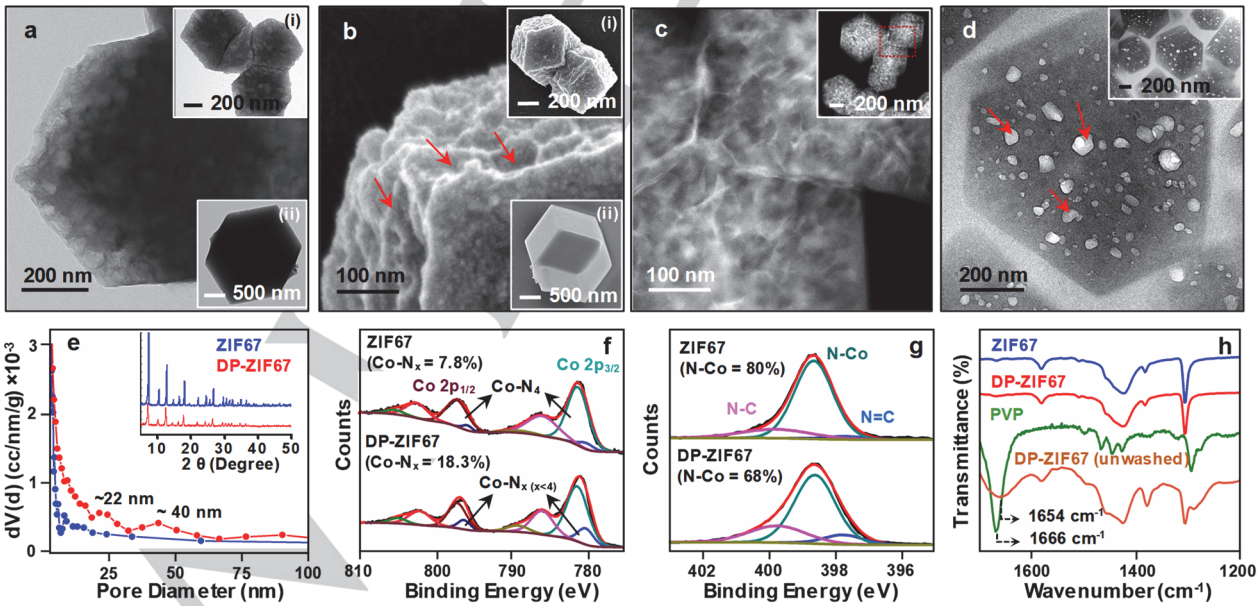

Figure 1. (a) TEM and (b) FESEM images of **DP-ZIF67**. Red arrows in panel b indicate the open pore structure in **DP-ZIF67**. Inset in panel (a) and (b) show low magnification TEM and FESEM images of **DP-ZIF67** (i) and **ZIF67** (ii). (c) HAADF-STEM image of **DP-ZIF67** (inset: low magnification image), (d) TEM image of **DP-ZIF67** after the treatment of focused ion beam (FIB) to visualize the cross section. Red arrows point out to the pores in dissected **DP-ZIF67** (inset: low magnification FIB-TEM image). (e) Pore size distribution plot and XRD pattern (inset) for **ZIF67** and **DP-ZIF67**. Deconvoluted XPS spectra of **ZIF67** and **DP-ZIF67** for (f) Co 2p (g) N 1s, (h) FTIR spectra for different samples.

10.1002/anie.201916578

795.5 eV are attributed to the unsaturated cobalt species in Co–N_x (x<4) geometry,[12] and the unsaturated Co sites present in **ZIF67** (7.8%) are significantly increased to 18.3% in case of **DP-ZIF67**. Moreover, the variation in deconvoluted N 1s XPS spectra is prominent for instance, the quantity of N-Co is considerably decreased from 80% in **ZIF67** to 68% in **DP-ZIF67** (Figure 1g), and thus corroborates the existence of large number of ligand-free unsaturated Co sites in **DP-ZIF67**. The thermogravimmetric analyses (TGA) patterns of **ZIF67** and **DP- ZIF67** were found to be identical showing ~42 and 40% weight loss, respectively, after heating at 800°C under N_2 gas environment; also both materials showed identical Fourier transform infrared (FTIR) spectra (Figure S9), where the characteristic – C=O stretching vibration corresponding to PVP at1666 cm^{-1} was absent, however the presence of peak at 1654 cm^{-1} (shifted to lower wave number from 1666 cm^{-1}) in the unwashed-**DP-ZIF67** (TEM image, Figure S10), could be ascribed to the feasible intermediates formation through coordination of Co(II) ions and carbonyl oxygen of PVP during the growth of **DP-ZIF67** crystal (Figure 1h), thereafter following the purification step, PVP unbinds and vanishes from the mesopores (Scheme S1). To demonstrate the generality of our approach, different type of mesoporous **ZIF8** (Zn-imidazole MOF), with large-sized pores was also synthesized (Figure S12c).

Next, with the intention of integrating catalytic functionality in the pores of MOFs, the pre-synthesized PVP-capped Pd NCs (2.6 ± 0.3 nm) were added to the precursor mixture while crystalizing the MOF, resulting the formation of Pd NCs stably and homogeneously encapsulated inside mesopores of **DP-ZIF67** (**Pd@DP-ZIF67**) (Figure 2a, S13, S14). The crystal structure of the hybrid material exhibited identical XRD diffraction patterns as that of **DP-ZIF67**, suggesting unaffected structural and composition of MOF after Pd NCs-functionalization (Figure S15a). Further, the HAADF-STEM image and EDS-elemental mapping confirmed the presence of Pd NCs with homogeneous distribution throughout the **DP-ZIF67** (Figure 2b). XPS analyses revealed high degree of unsaturation in Co sites (Co-N_x = 17.3%, N-Co = 71%) in **Pd@DP-ZIF67** similar to the parent **DP-ZIF67** (Figure S15b, c), with the presence of dominating Pd(0) species. Similarly, we also synthesized **Pt@DP-ZIF67** by introducing PVP capped Pt NCs (Figure S17); and by sequentially adding different metal NCs, hierarchically segregated core@shell-type distribution of different metal NCs was also realized within **DP-ZIF67** crystal (namely, **Pt_{Core}/Pd_{Shell}@DP-ZIF67** (Figure 2c). Further, with the intention of advancing **Pd@DP-ZIF67** for targeted chemo-biocatalytic cascade reactions, additional inclusion of large-sized biocatalysts was attempted, where the large mesoporous channels (20-40 nm) with open apertures within MOF-architecture can encapsulate and stabilize the enzymes and then interconnected MOF-microchannels can effectively permit the reactant/product transport. For this, **Pd@DP-ZIF67** was incubated with *Candida antractica* lipase A (CalA; *ca*. 6.3 × 5.6 × 4.2 nm in size), where the amount of final loaded enzyme was 26.5% as measured by Bradford assay (inset; Figure 2e, S18), and the FTIR spectrum of **Pd@DP-ZIF67/CalA** exhibited C=O stretching vibration for amide-I of the enzyme at 1660 cm^{-1}, along with other characteristic peaks for **ZIF67** (Figure 2f). The enzyme content in **Pd@DP-ZIF67/CalA** was also verified by inductively coupled plasma optical emission spectrometry (ICP-OES) measurement of S (cysteine residues in CalA) (Table S1). TEM and XRD analyses of the **Pd@DP-ZIF67/CalA** illustrated the well-maintained crystalline structure and morphology of the MOF, with evenly dispersed Pd NCs and enzymes, as also confirmed from HAADF-STEM and EDS-mapping analysis (Figure 2d, S19). Notably, the incorporation of Pd NCs into the pores of MOFs reduces the available pore size of DP-ZIF67 as verified from the BJH plot of **Pd@DP-ZIF67**, which has been reflected in lowered CalA loading capacity compared to **DP-ZIF67**, but still possesses large-sized pores (5-17 nm) for high quantity of enzyme encapsulation (Figure 2e). Furthermore, after enzyme encapsulation, BJH analysis of **Pd@DP-ZIF67/CalA** showed absence of large mesopores, which inferred enzymes, occupied the mesopores of **DP-ZIF67** while retaining unsaturated Co centers as confirmed from XPS (Figure 3e, S19, S20).

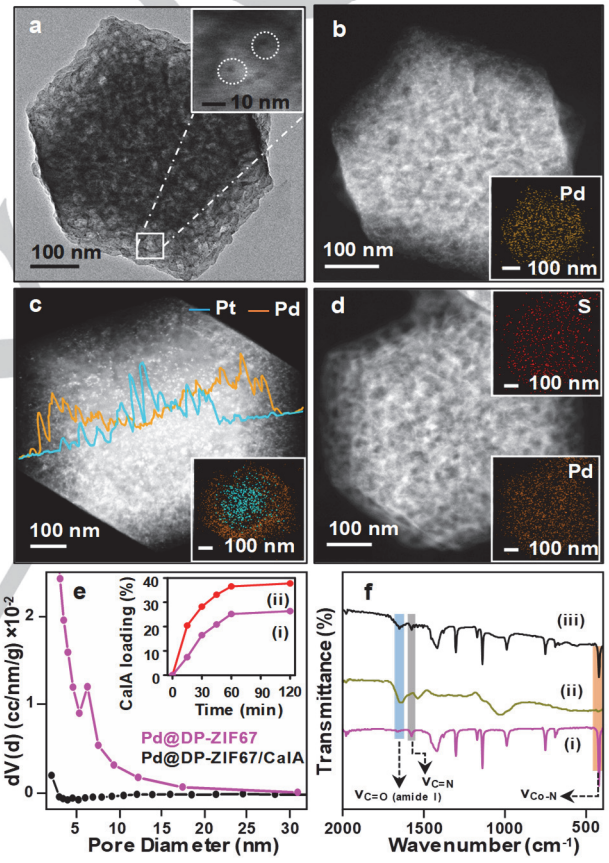

Figure 2. (a) TEM image and HRTEM image (inset), (b) HAADF-STEM and EDS mapping of Pd (inset) of **Pd@DP-ZIF67**. HAADF-STEM and EDS mapping (inset) of (c) **Pt_{Core}/Pd_{Shell}@DP-ZIF67** and (d) **Pd@DP-ZIF67/CalA**. (e) Pore size distribution plot of **Pd@DP-ZIF67** and **Pd@DP-ZIF67/CalA**: inset shows enzyme encapsulation kinetics for various substrates such as **Pd@DP-ZIF67** (i), and **DP-ZIF67** (ii). (f) FTIR spectra for **Pd@DP-ZIF67** (i), CalA (ii), and **Pd@DP-ZIF67/CalA** (iii).

We envisioned **Pd@DP-ZIF67/CalA** to be multimodal catalytic platform for carrying out such cascade reactions, where unsaturated metallic nodes of MOF acting as Lewis acidic catalytic sites for nitroaldol reaction, Pd-NCs as racemization catalyst and CalA for enzymetic kinetic resolution coexist within a

10.1002/anie.201916578

WILEY-VCH

COMMUNICATION

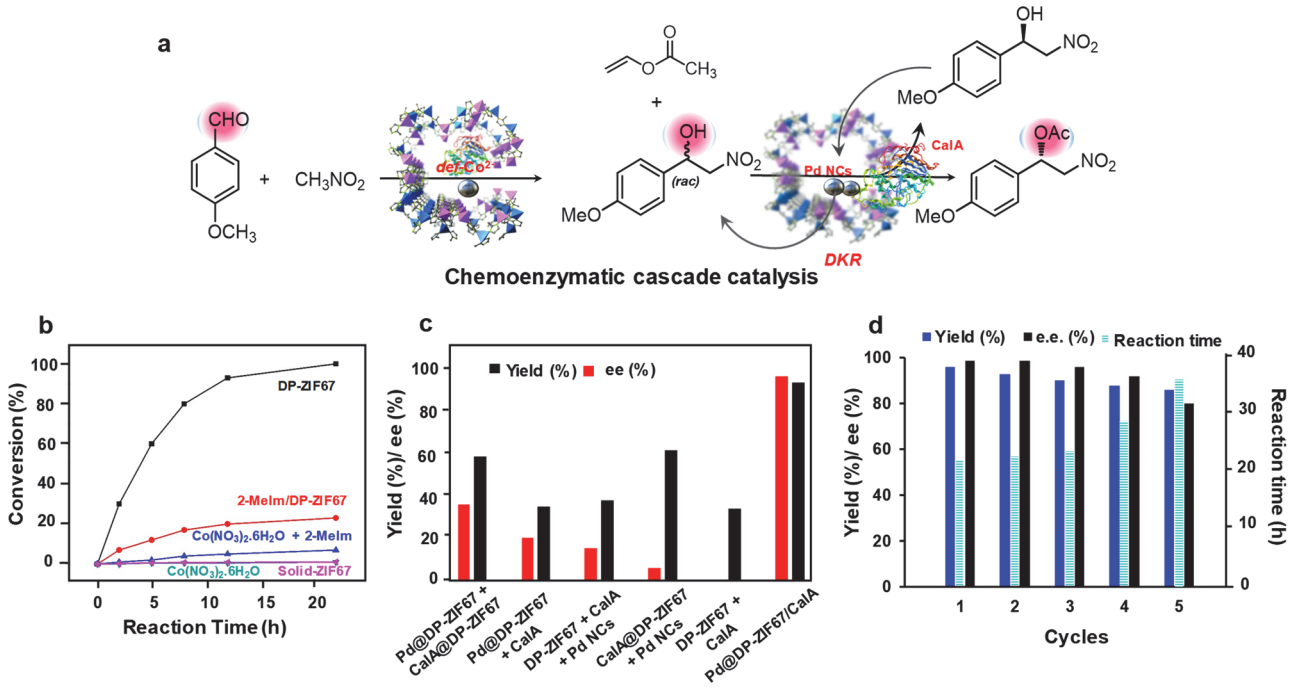

e

S. No.	Starting Material	Product	Conversion (%)	Yield (%)	ee (%)	Reaction Time (h)
1.	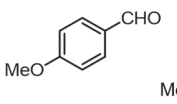	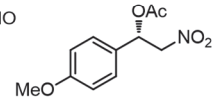	>99	~96	>99	20
2.	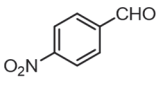	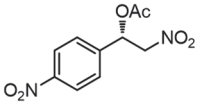	>99	~99	>99	20
3.	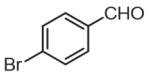	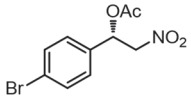	>99	~99	>99	21
4.	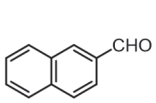	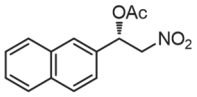	>99	~99	>99	22
5.	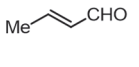	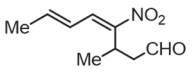	>99	~80	NA	30

Figure 3. (a) Schematic illustration of the cascade reaction catalyzed by **Pd@DP-ZIF67/CalA**, (b) Kinetics of nitrol-aldol reaction catalyzed by **DP-ZIF67** and various control catalysts. (c) The **Pd@DP-ZIF67/CalA** and various control catalysts catalyzed cascade catalysis to obtain enantiomerically pure β-nitroacetate, in high yield showing the co-immobilization of the catalysts has immense effect on the product enantiomeric excess (ee) and yield of the product. (d) Reaction yield, ee values and time of five cycles using **Pd@DP-ZIF67/CalA** as the catalyst for the conversion of *p*-anisaldehyde to β-nitroacetate product. (e) Substrate scopes of cascade nitro aldol followed by dynamic kinetic resolution of various aldehydes.

single nanoreactor space, which can carry out all chemo-enzymatic steps efficiently and synergistically. To evaluate the catalytic performance of **Pd@DP-ZIF67/CalA**, the nitroaldol reaction (Henry reaction) catalyzed by unsaturated cobalt(II) sites[13] of ZIF67 followed by the Pd NCs-catalyzed racemization of resulting secondary nitro alcohol which was coupled with lipase catalyzed acylation of alcohol in one-pot cascade manner, was chosen.[14] After optimizing the reaction conditions (Table S2), we conducted the cascade reaction in THF:toluene (4:1) solvent at r.t. with *p*-anisaldehyde and nitromethane using 0.1 mol% *N*,*N*-diisopropylethylamine and vinylacetate as the acyl donor in the presence of the **Pd@DP-ZIF67/CalA** (Figure 3), to obtain desired enantiopure chiral acetylated nitroalcohol, with >97% conversion yield (Figure S22) and an >99% enantiomeric excess (>99% ee),

10.1002/anie.201916578

with a substrate concentration of 1 mM (Figure S23). To verify the high activity of defect rich site of Co(II) in **DP-ZIF67** for nitroaldol reaction, control experiments, with $Co(NO_3)_2{\cdot}6H_2O$, mixture of $Co(NO_3)_2{\cdot}6H_2O$ and imidazole, and solid **ZIF67** displayed very poor catalytic reactivities compared to the **DP-ZIF67** (Figure 3b). Interestingly, **DP-ZIF67** pre-treated with excess ligand (2-methylimidazole, 2-MeIm) afforded poor yield of the nitroaldol product due to the saturation of catalytic Co(II) sites by 2-MeIm, suggesting the crucial role of uncoordinated Co(II) sites present in the mesoporous morphology (Figure 3b, S24). Further to prove the efficacy of our integrated multimodal catalytic platform, the physical mixture of **DP-ZIF67**, **PdNCs** and CalA afforded only *ca.* 20% ee; similarly, the physical mixture of **Pd@DP-ZIF67** and **CalA@DP-ZIF67** also provided very poor ee (*ca.* 38%) of the nitroacetate product. In another control experiment, physical mixture of **Pd@DP-ZIF67** and free CalA for cascade catalysis resulted only *ca.* 24% ee of the product, inferring that immobilization of CalA in MOF mesopores could not only increase the stability and active sites exposure of enzyme in spite of being in non-polar organic solvent, but also locally provide enhanced substrate concentration for kinetic resolution step. In all these control experiments, the lower yields (35-63%) (Figure S25-26) of nitroacetates also corroborated the advantage of integrated design resulting in to the high reactivity of **Pd@DP-ZIF67/CalA**. Above control experiments (Figure 3c) where isolating PdNCs or CalA from MOF and adding them as a physical mixture, afforded much inferior yields and enantioselectivities due to the possible side-reactions and deactivation of isolated enzymes and PdNCs. These observations can rationalize the importance of ingeniously integrated design of the catalyst where three chemo- & bio-catalytic modules function in a synergistic fashion much superior to the isolated catalytic entities added as the physical mixtures: implementing to a nitroaldol-DKR-esterification cascade reaction, mesoporous MOF nano-housing having massively uncoordinated metal nodes, activates aldehyde-substrate generating nitroalcohols concentrated locally within the vicinity of well-protected PdNCs and enzymes for successive highly efficient reversible-DKR and esterification reaction due to the confined nanoscale proximities of the three catalytic entities.[3a,15] Additionally, the **Pd@DP-ZIF67/CalA** were easily recovered by centrifugation after the reaction (Figure 3d) and exhibited moderately affected (>89%) residual activity, affording 86% yield and >80% ee of product after five successive recycling-steps. Although, the reaction time was found to be consistent up to 2nd cycle, while in the next cycles, slight longer reaction times (3rd cycle: 24 h, 4th cycle 28 h, 5th cycle: 35 h) were noticed. Further the TEM, HRTEM, HAADF-STEM, EDS mapping analyses after each catalytic cycle revealed no significant change in the morphology of the ZIF67, PdNCs and CalA loading and their aggregation up to 5th cycle (Figure S27-S31), however ICP analyses revealed the loss of some Pd and S contents after 4th and 5th cycles (Figure S32). After 5th catalytic cycle the reappearance of mesopores in BJH analyses also suggested the possible detachment of CalA and Pd NCs from the MOF as shown in Figure S33. Further, the scope of **Pd@DP-ZIF67/CalA** was extended to the differently substituted aryl and aliphatic aldehydes. As shown in Figure 3e, the **Pd@DP-ZIF67/CalA** afforded excellent yields (>99%) and ee (>99%) of the desired nitroacetates in the case of different substituted aryl aldehydes (entry 1-4) (Figure S34-39) without showing any significant electronic effect of substituents; whereas, in the case of crotonaldehyde, the expected nitroacetate product could not be isolated, due to the *in situ* conversion to a different product as characterized from NMR spectroscopy (entry 5) (Figure S40-41).

In conclusion, we devised a synthetic strategy to construct ultra-large mesopores (20-40 nm) in MOF-crystals with the aid of competitive coordination chemistry by metallophilic polymer (PVP) and ingeniously integrated different catalytic modalities: coordinatively unsaturated metal cations as Lewis acids-, heterogeneous metal NCs- and enzyme-based catalysis within a single mesoporous MOF-nanohousing. Such proximal engineering of different catalytic functionalities in single MOF-nanoplatform can synergistically perform multistep divergent cascade reactions under ambient conditions — nucleophilic addition, chiral center generation, racemization and kinetic resolution, affording final product in excellent yields and enantiomeric excess. Present work would lead to the revenues in overcoming drawbacks and blurring the divisions and limitations of conventional homogeneous, heterogeneous and biocatalytic platforms.

Acknowledgements

This work was supported by the Basic Science Research Program through the National Research Foundation of Korea (NRF) funded by the Ministry of Science, ICT & Future Planning (MSIP) (Grant NRF-2016R1A3B1907559) (I.S.L.). We would like to thank Dr. Jin Young Koo and Prof. Hee Cheul Choi for helpful discussion.

Keywords: nanocatalyst • mesoporous MOF • cascade reaction • multimodal catalyst • chemo-bio-catalyst

[1] R. Ye, J. Zhao, B. B. Wickemeyer, F. D. Toste, G. A. Somorjai, *Nat. Catal.* **2018**, *1*, 318–325.

[2] a) F. Rudroff, M. D. Mihovilovic, H. Gröger, R. Snajdrova, H. Iding, U. T. Bornscheuer, *Nat. Catal.* **2018**, *1*, 12–22; b) C. A. Denard, J. F. Hartwig, H. Zhao, *ACS Catal.* **2013**, *3*, 2856–2864.

[3] a) K. Engström, E. V. Johnston, O. Verho, K. P. J. Gustafson, M. Shakeri, C.-W. Tai, J.-E. Bäckvall, *Angew. Chem. Int. Ed.* **2013**, *52*, 14006 – 14010; b) H. Deng, S. Grunder, K. E. Cordova, C. Valente, H. Furukawa, M. Hmadeh, F. Gandara, A. C. Whalley, Z. Liu, S. Asahina, H. Kazumori, M. O'Keeffe, O. Terasaki, J. F. Stoddart, O. M. Yaghi, *Science* **2012**, *336*, 1018–1023; c) W. Xu, Z. Fu, G. Chen, Z. Wang, Y. Jian, Y. Zhang, G. Jiang, D. Lu, J. Wu, Z. Liu, *Nat. Commun*. **2019**, *10*, 2684; d) X. Li, Y. Cao, K. Luo, Y. Sun, J. Xiong, L. Wang, Z. Liu, J. Li, J. Ma, J. Ge, H. Xiao, R. N. Zare, *Nat. Catal.* **2019**, *2*, 718–725.

[4] R. Chapman, M. H. Stenzel, *J. Am. Chem. Soc.* **2019**, *141*, 2754−2769.

[5] a) Q. Yang, Q. Xu, H.-L. Jiang, *Chem. Soc. Rev.* **2017**, *46*, 4774−4808; b) X. Li, B. Zhang, L. Tang, T. W. Goh, S. Qi, A. Volkov, Y. Pei, Z. Qi, C.-K. Tsung, L. Stanley, W. Huang. *Angew. Chem. Int. Ed.* **2017**, *56*, 16371–16375; c) H. Kobayashi, Y. Mitsuka, H. Kitagawa, *Inorg. Chem.* **2016**, *55*, 7301−7310; d) Q.-L. Zhu, J. Li, Q. Xu, *J. Am. Chem. Soc.* **2013**, *135*, 10210−10213; e) G. Lu, S. Li, Z. Guo, O. K. Farha, B. G. Hauser, X. Qi, Y. Wang, X. Wang, S. Han, X. Liu, J. S. DuChene, H. Zhang, Q. Zhang, X. Chen, J. Ma, S. C. J. Loo, W. D. Wei, Y. Yang, J. T. Hupp, F. Huo, *Nat. Chem.* **2012**, *4*, 310– 316; f) C.-H. Kuo, Y. Tang, L.-Y. Chou, B. T. Sneed, C. N. Brodsky, Z. Zhao, C.-K. Tsung, *J. Am. Chem. Soc.* **2012**, *134*, 14345−14348; g) V. Pascanu, G. G. Miera, A. K. Inge, B. Mañtin-Matute, *J. Am. Chem. Soc.* **2019**, *141*, 7223−7234.

10.1002/anie.201916578

[6] a) J. Zhuang, A. P. Young, C.-K. Tsung, *Small* **2017**, *13,* 1700880; b) P. Li, S. Y. Moon, M. A. Guelta, S. P. Harvey, J. T. Hupp O. K., Farha, *J. Am. Chem. Soc.* **2016**, *138*, 8052−8055.

[7] a) P. Liu, E. Redekop, X. Gao, W.-C. Liu, U. Olsbye, G. A. Somorjai, *J. Am. Chem. Soc.* **2019**, *141*, 11557−11564; b) H.-Y. Guan, R. J. LeBlanc, S.-Y. Xie, Y. Yue, *Coord. Chem. Rev.* **2018**, *369*, 76–90.

[8] a) D. Feng, T.-F. Liu, J. Su, M. Bosch, Z. Wei, W. Wan, D. Yuan, Y.-P. Chen, X. Wang, K. Wang, X. Lian, Z.-Y. Gu, J. Park, X. Zou, H.-C. Zhou, *Nat. Commun.* **2015**, *6*, 5979; b) Y. Chen, S. Han, X. Li, Z. Zhang, S. Ma, *Inorg. Chem.* **2014**, *53*, 10006−10008.

[9] a) S. Yuan, L. Zou, J.-S. Qin, J. Li, L. Huang, L. Feng, X. Wang, M. Bosch, A. Alsalme, T. Cagin, H.-C. Zhou, *Nat. Commun.* **2017**, *8*, 15356; b) A. J. Rieth, Y. Tulchinsky, M. Dincă, *J. Am. Chem. Soc.* **2016**, *138*, 9401−9404; c) H.-Y. Ren, R.-X. Yao, X.-M. Zhang, *Inorg. Chem.* **2015**, *54*, 6312−6318; d) Z. Fang, J. P. Dürholt, M. Kauer, W. Zhang, C. Lochenie, B. Jee, B. Albada, N. Metzler-Nolte, A. Pöppl, B. Weber, M. Muhler, Y. Wang, R. Schmid, R. A. Fischer, *J. Am. Chem. Soc.* **2014**, *136*, 9627−9636; e) D. J. Xiao, E. D. Bloch, J. A. Mason, W. L. Queen, M. R. Hudson, N. Planas, J. Borycz, A. L. Dzubak, P. Verma, K. Lee, F. Bonino, V. Crocella, J. Yano, S. Bordiga, D. G. Truhlar, L. Gagliardi, C. M. Brown, J. R. Long, *Nat. Chem.* **2014**, *6*, 590–595.

[10] a) P. Li, J. A. Modica, A. J. Howarth, E. L. Vargas, P. Z. Moghadam, R. Q. Snurr, M. Mrksich, J. T. Hupp, O. K. Farha, *Chem.* **2016**, *1*, 154–169; b) V. Lykourinou, Y. Chen, X.-S. Wang, L. Meng, T. Hoang, L.-J. Ming, R. L. Musselman, S. Ma, *J. Am. Chem. Soc.* **2011**, *133*, 10382–10385.

[11] a) F. Meng, S. Zhang, L. Ma, W. Zhang, M. Li, T. Wu, H. Li, T. Zhang, X. Lu, F. Huo, J. Lu, *Adv. Mater.* **2018**, *30*, 1803263; b) G. Cai, H.-L. Jiang, *Angew. Chem. Int. Ed.* **2017**, *56*, 563–567; c) W. Zhang, Y. Liu, G. Lu, Y. Wang, S. Li, C. Cui, J. Wu, Z. Xu, D. Tian, W. Huang, J. S. DuCheneu, W. D. Wei, H. Chen, Y. Yang, F. Huo**,** *Adv. Mater.* **2015,** *27*, 2923–2929; d) L.-B. Sun, J.-R. Li, J. Park, H.-C. Zhou, *J. Am. Chem. Soc.* **2012**, *134*, 126−129; e) G. C. Shearer, S. Chavan, S. Bordiga, S. Svelle, U. Olsbye, K. P. Lillerud, **2016**, *28*, 3749−3761.

[12] L. Tao, C.-Y. Lin, S. Dou, S. Feng, D. Chen, D. Liu, J. Huo, Z. Xia, S. Wang, *Nano Energy* **2017**, *41*, 417–425.

[13] J. Park, K. Lang, K. A. Abboud, S. Hong, *J. Am. Chem. Soc.* **2008**, 130, 16484–16485.

[14] a) O. Verho, J.-E. Bäckvall, *J. Am. Chem. Soc.* **2015**, *137*, 3996−4009; b) T. Langvik, O. Saloranta, D. Y. Murzin, R. Leino, *ChemCatChem* **2015**, *7*, 4004 – 4015.

[15] Y. Xu, M. Wang, B. Feng, Z. Li, Y. Li, H. Li, H. Li, *Catal. Sci. Technol.* **2017**, *7*, 5838–5842.

10.1002/anie.201916578

WILEY-VCH

Entry for the Table of Contents (Please choose one layout)

COMMUNICATION

A multimodal catalytic nanoreactor consisting of metal nanocrystals, stably anchored enzymes and coordinatively unsaturated metal nodes inside the mesopores of metal organic framework is established to accomplish one-pot multi-step cascade reactions.

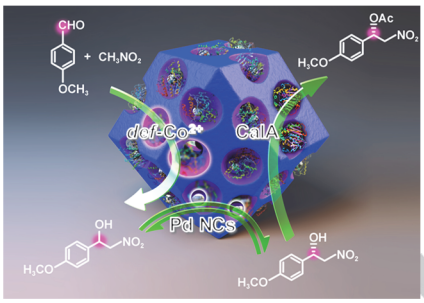

*Soumen Dutta, Nitee Kumari, Sateesh Dubbu, Sun Woo Jang, Amit Kumar, Hiroyoshi Ohtsu, Junghoon Kim, Seung Hwan Cho, Masaki Kawano, and In Su Lee**

Page No. – Page No.

Highly Mesoporous Metal Organic Frameworks as Synergistic Multimodal Catalytic Platforms for Divergent Cascade Reactions